

**Conical dispersion of Lamb waves in elastic plates**

David M. Stobbe and Todd W. Murray\*

*Department of Mechanical Engineering, University of Colorado at Boulder, Boulder, Colorado 80309, USA*

(Received 29 June 2017; revised manuscript received 28 August 2017; published 4 October 2017)

Guided elastic waves in homogeneous isotropic plates exhibit conical dispersion at zero wave number for discrete values of Poisson's ratio where accidental degeneracy between longitudinal and transverse thickness resonances occur. Waves excited at the coincidence frequency have the infinite phase velocity associated with thickness mode resonances, but the group velocity remains finite. This leads to propagating waves that oscillate in time but are spatially uniform over the plate surface. Here, accidental degeneracy is induced in an aluminum plate by cooling the plate to tune the Poisson's ratio through the degenerate point. We measure linear dispersion in the transition from forward to backward propagating waves near zero wave number. In addition, we demonstrate that waves generated near the coincidence frequency exhibit spatially uniform phase over the plate surface, and show angle independent mode conversion upon encountering the free edge of the plate. We propose that elastic plates offer a simple system to explore the physics of conical dispersion at zero wave number, and that this phenomenon may find application in acoustic devices and nondestructive testing.

DOI: [10.1103/PhysRevB.96.144101](https://doi.org/10.1103/PhysRevB.96.144101)**I. INTRODUCTION**

Guided elastic waves that propagate in plates, or Lamb waves, have been studied extensively and used for a variety of applications in materials characterization and nondestructive testing [1,2]. Recently, there has been an interest in utilizing some of the peculiar properties of Lamb waves for enhanced nondestructive testing of materials and for the manipulation of wave fields in novel ways. Lamb waves are dispersive and the propagating modes within a given plate are dictated by the mechanical properties of the plate and are represented by a dispersion curve giving the frequency ( $\omega$ ) as a function of wave vector ( $k$ ). For some Lamb wave modes, the curvature of the dispersion near  $k = 0$  is negative, leading to a region of backward wave propagation over which the phase velocity and group velocity are antiparallel [3,4]. These modes also exhibit a point where the group velocity goes through zero, while the phase velocity remains finite, in the transition from backward to forward wave propagating modes. Such zero group velocity (ZGV) points exhibit a strong resonance that can be efficiently generated with a laser excitation source, and they have been used for a variety of applications in the nondestructive evaluation of materials [5–9]. In addition, it has been demonstrated that the mode conversion between backward and forward propagating Lamb waves at a thickness step in a plate or at a plate edge gives rise to nonintuitive effects such as negative refraction and negative reflection [10–14].

The origin of backward wave propagation in both elastic and optical waveguides lies in the repulsion of the dispersion curves between modes of the same symmetry [8,15]. This repulsion is the strongest when an accidental degeneracy, dictated by the material properties rather than symmetry, occurs between closely spaced modes. For isotropic plates, the Poisson's ratio (or alternatively, ratio of the bulk wave velocities) determines the character of dispersion. The dispersion curves intersect the  $k = 0$  axis at the thickness mode resonances, where the phase velocity becomes infinite while

the group velocity vanishes. The dispersion curve is generally parabolic in the long-wavelength limit as is dictated by the requirement that  $\omega(k) = \omega(-k)$ . If, however, the Poisson's ratio is selected such that an accidental degeneracy occurs between a longitudinal thickness mode resonance and a shear thickness mode resonance, of the same symmetry, then the dispersion curve becomes linear in the vicinity of  $k = 0$  and, in a three-dimensional representation, assumes the shape of a cone [16]. This conical dispersion of Lamb waves for special values of Poisson's ratio was originally described mathematically by Mindlin more than a half of a century ago [17].

More recently, there has been considerable interest in both the photonics and acoustics communities in the development of metamaterials that exhibit conical dispersion at  $k = 0$  [18–26]. This is typically referred to as Dirac cone or Dirac-like cone dispersion depending on the characteristics of the degeneracy that occurs. Maznev recently highlighted the similarities (and differences) between conical dispersion in isotropic plates and metamaterials [27]. A salient feature of conical dispersion at  $k = 0$  is that the phase velocity is infinite, while the group velocity remains finite. As the wavelength is infinite, conical dispersion at  $k = 0$  essentially decouples the spatial and temporal behavior of the wave field and produces a field that is static in space yet oscillating in time. In terms of metamaterials, it has been shown that conical dispersion at  $k = 0$  can be used to manipulate wave fields in novel ways to produce effects including tunneling, beam steering, total reflection, cloaking, and lensing [18–26].

While there has been intensive development in designer materials that have conical dispersion at  $k = 0$ , the study of this phenomena in isotropic plates has been limited. In fact, there have been no experimental investigations of conical or near-conical dispersion of Lamb waves in isotropic plates near  $k = 0$ , or the unusual physical phenomena associated with such waves, reported in the literature. In part, this may be due to the fact that accidental degeneracy only occurs at distinct values of Poisson's ratio. In this paper, we report the experimental measurement of linear dispersion through  $k = 0$  in a homogeneous isotropic plate. Starting with an

\*todd.murray@colorado.edu

aluminum alloy plate with a near degeneracy, we slightly modify the elastic properties through temperature change to achieve degeneracy at  $k = 0$ . Furthermore, we demonstrate the spatial and temporal decoupling of Lamb waves with near-conical dispersion through experiments showing angle invariant mode conversion from the free edge of a plate.

## II. CONICAL DISPERSION OF LAMB WAVES

For freestanding plates, longitudinal and transverse thickness mode resonances occur at  $k = 0$ . These result in symmetric or antisymmetric wave fields with respect to the midplane of the plate. The resonance frequencies and symmetries of the oscillations are [17]

$$\begin{aligned} \omega_{m,L}^0 &= \frac{\pi m c_1}{h} \begin{pmatrix} m = 1, 3, 5\dots & \text{symmetric} \\ m = 2, 4, 6\dots & \text{antisymmetric} \end{pmatrix}, \\ \omega_{n,T}^0 &= \frac{\pi n c_2}{h} \begin{pmatrix} n = 1, 3, 5\dots & \text{antisymmetric} \\ n = 2, 4, 6\dots & \text{symmetric} \end{pmatrix}. \end{aligned} \quad (1)$$

Here  $c_1$  and  $c_2$  are the longitudinal ( $L$ ) and transverse ( $T$ ) wave velocities, respectively, and  $h$  is the plate thickness. The cutoff frequencies for longitudinal resonances give rise to symmetric modes if  $m$  is odd and antisymmetric modes if  $m$  is even, while the opposite is true for the transverse resonances. In the vicinity of  $k = 0$ , the dispersion branches can generally be found by expanding  $\omega(k)$  in even powers of  $k$  giving [28]

$$\omega_{m,\alpha}(k) = \omega_{m,\alpha}^0 + \frac{1}{2} \left( \frac{\partial^2 \omega_{m,\alpha}}{\partial k^2} \right)_{k=0} k^2 + O(k^4), \quad (2)$$

where  $\alpha$  corresponds to either a longitudinal or transverse resonance and the curvatures in the long-wavelength limit are given by

$$\begin{aligned} \left( \frac{\partial^2 \omega_{m,L}}{\partial k^2} \right) &= \frac{c_1 h}{\pi m} + \frac{16 h c_2^3}{\pi^2 m^2 c_1^2} \tan \left[ \frac{\pi m}{2} \left( 1 - \frac{c_1}{c_2} \right) \right], \\ \left( \frac{\partial^2 \omega_{n,T}}{\partial k^2} \right) &= \frac{c_2 h}{\pi n} + \frac{16 h c_1^2}{\pi^2 n^2 c_2} \tan \left[ \frac{\pi n}{2} \left( 1 - \frac{c_2}{c_1} \right) \right]. \end{aligned} \quad (3)$$

The first term in the curvature equations is always positive, while the second term can take on positive or negative values for a given mode depending on the Poisson's ratio. This term is associated with the interaction between mode curves in the plate. The tangent term becomes infinite, and the interaction strongest, only in cases where the ratio of the wave velocities is equal to the irreducible ratio of two positive integers of different parity (one odd and one even) [28]. This is precisely the condition for the occurrence of degeneracy between longitudinal and transverse thickness resonances of the same symmetry. For example, if the ratio between longitudinal and shear wave velocities is equal to two, the first longitudinal resonance ( $m = 1$ ) and the second transverse resonance ( $n = 2$ ) occur at the same frequency. In fact, this case results in degeneracies between odd  $m$ -order longitudinal resonances and  $2m$ -order transverse resonances of the same symmetry. We note that degeneracy between modes of opposite symmetry does not lead to a divergence in the interaction term or conical dispersion.

In the case in which the interaction term in Eq. (3) goes to infinity, the quadratic dispersion indicated by Eq. (2) is no

longer valid. As shown by Mindlin, the slope is nonzero at  $k = 0$  and the local dispersion assumes the linear of the form [17]

$$\omega_{m,\alpha}(k) = \omega_{m,\alpha}^0 \pm \left( \frac{\partial \omega_{m,\alpha}}{\partial k} \right)_{k=0} k, \quad (4)$$

where the group velocity is given by

$$v_g = \left( \frac{\partial \omega_{m,\alpha}}{\partial k} \right)_{k=0} = \frac{4c_2}{\pi n}, \quad n = 2, 3, 4, \dots \quad (5)$$

In such case, the dispersion curves consist of two lines intersecting at the coincidence frequency at  $k = 0$ , with the line segments above  $\omega_{m,\alpha}^0$  exhibiting forward wave propagation, and the line segments below showing backward wave propagation. An example of conical dispersion of Lamb waves with  $c_1 = 2c_2$  ( $h = 1.532$  mm,  $c_2 = 3.138$  mm/ $\mu$ s) is given in Fig. 1(a). Here, the  $S_2/S_{2B}$  modes and  $S_5/S_{5B}$  modes are degenerate at  $k = 0$ , leading to linear dispersion in the long-wavelength limit. A zoomed-in view of the  $S_2/S_{2B}$  modes for the degenerate case, along with a near-degenerate case, is shown in Fig. 1(b). Generally, the forward propagating branch is referred to as the  $S_2$  mode, while the backward propagating branch is referred to as the  $S_{2B}$  mode. Note that the forward and backward propagating branches are actually both part of the same continuous  $S_2$  mode and are connected to each other (in the absence of degeneracy) through a loop in the imaginary ( $\omega, k$ ) plane. In Fig. 1(b), the solid line indicates the dispersion curve associated with waves propagating in the (arbitrarily defined) positive direction, while the dotted lines indicate the curve associated with waves propagating in the opposite direction. In the case of degeneracy, the imaginary loop between the  $S_2$  and  $S_{2B}$  branches is closed, resulting in a smooth transition of the  $S_2$  mode through  $k = 0$ . Equation (4) indicates two lines in the degenerate case, ensuring that  $\omega(k) = \omega(-k)$  is satisfied. In general, conical dispersion of Lamb waves is associated with closing the imaginary loop of individual modes that exhibit both longitudinal and shear thickness resonances.

In order to demonstrate the excitation of Lamb waves near the conical point, the integral transform technique [29] was used to calculate the response of a 1.0-mm-thick plate to a normal force with a Gaussian spatial distribution with a full width at half maximum (FWHM) of 12.5 mm. The temporal profile of the source was also Gaussian with a FWHM of 10 ns, and the wave speeds were selected as  $c_1 = 6.0$  and  $c_2 = 3.0$  mm/ $\mu$ s ( $\nu = 1/3$ ). The calculated time domain displacement fields were bandpass filtered between 2.0 and 4.0 MHz to isolate the  $S_2/S_{2B}$  mode near the degeneracy at 3.0 MHz. The resulting waveforms, giving the normal displacement as a function of time at several source-to-receiver distances, are shown in Fig. 2(a). The time domain responses show the arrival of an initial wave packet that propagates with little distortion, followed by a sustained surface oscillation. The magnitude of the Fourier transform of the waveform calculated for a source-to-receiver distance of 30 mm is shown in Fig. 2(b). This spectrum has strong peaks both above (forward propagating waves) and below (backward propagating waves) the conical point with a dip occurring at

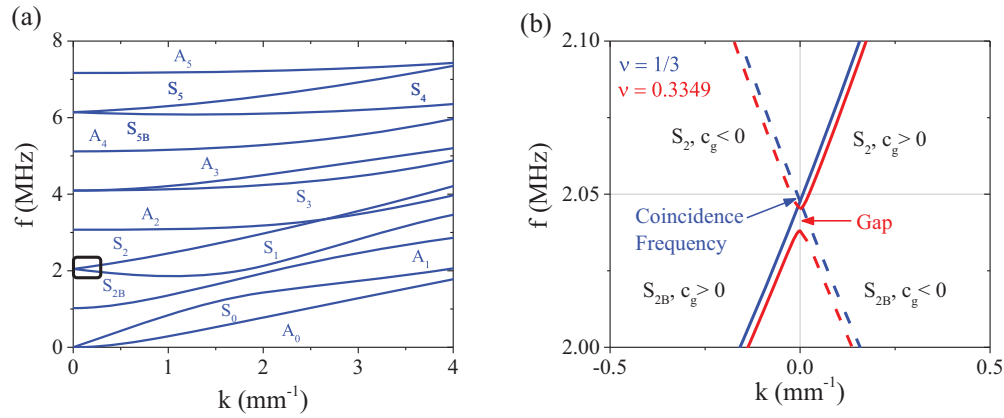


FIG. 1. (a) Dispersion curve for a plate with  $\nu = 1/3, h = 1.532 \text{ mm}, c_2 = 3.138 \text{ mm}/\mu\text{s}$ . The  $S_2/S_{2B}$  and  $S_5/S_{5B}$  modes are each degenerate at  $k = 0$  and show linear dispersion in the long-wavelength limit. (b) Zoomed-in portion of the dispersion curve shown in (a) near the lowest frequency degenerate point where longitudinal and transverse resonance frequencies associated with the  $S_2/S_{2B}$  modes are coincident (blue). Also shown is a near-degenerate case (corresponding to aluminum alloy 6061-0 at room temperature) with  $\nu = 0.3349, h = 1.533 \text{ mm}$ , and  $c_2 = 3.125 \text{ mm}/\mu\text{s}$ . Here  $c_g$  is the group velocity.

the coincidence frequency. The initial wave packets in the time domain are composed of forward and backward propagating waves in the nearly linear dispersion region close to  $k = 0$ .

After these wave packets pass the observation point, the surface continues to oscillate. Figure 2(c) shows a zoomed-in view of the surface displacements at all source-to-receiver distances

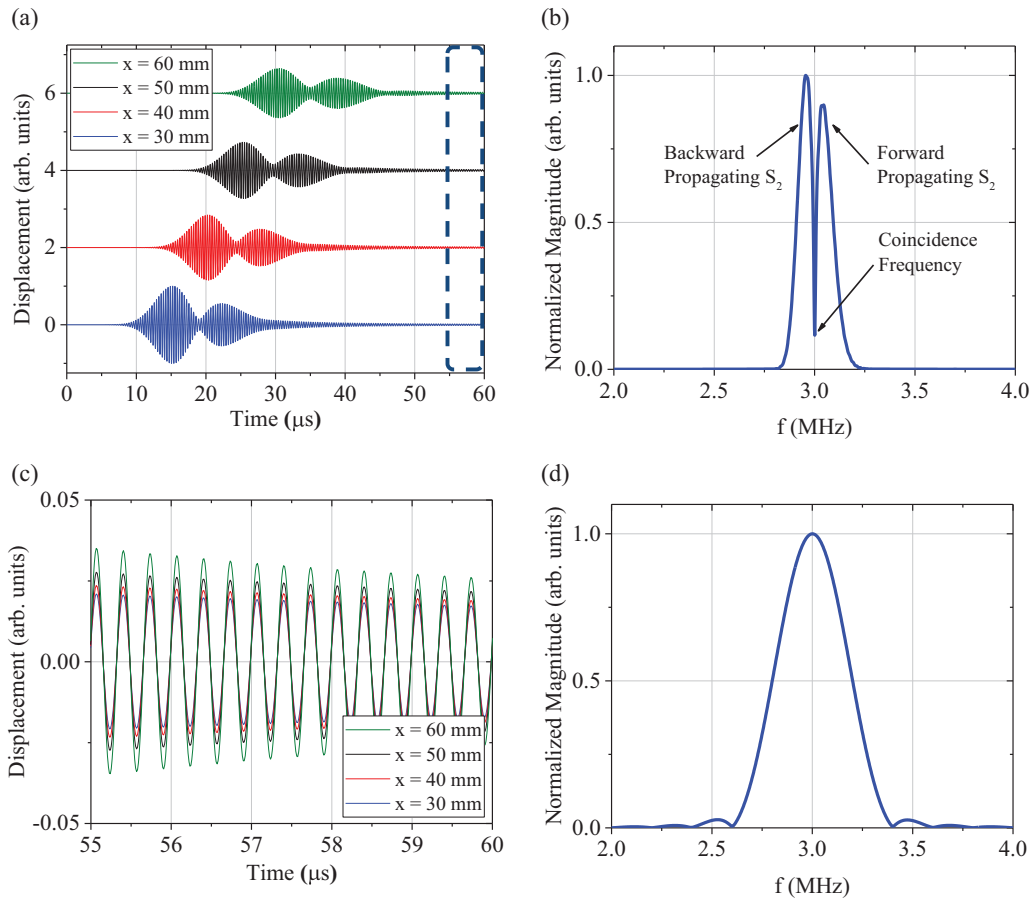


FIG. 2. (a) Calculated surface normal displacement of a plate in response to a surface normal force. The plate has a thickness of 1 mm and the wave velocities are taken as  $c_1 = 6.0 \text{ mm}/\mu\text{s}$  and  $c_2 = 3.0 \text{ mm}/\mu\text{s}$ . Wave forms are shown for several source-to-receiver distances. (b) Magnitude of the Fourier transform of the wave form calculated at a source-to-receiver distance of 30 mm. (c) Zoomed-in portion of the wave forms shown in (a) showing the uniform phase of the surface oscillations. (d) Magnitude of the Fourier transform of the wave form calculated at a source-to-receiver distance of 30 mm and time windowed between 55 and 60  $\mu\text{s}$ .

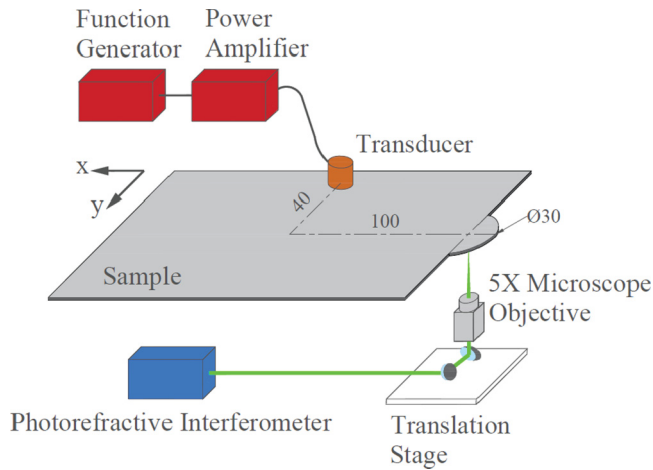


FIG. 3. Schematic of experimental setup for generating and detecting Lamb waves with conical and near-conical dispersion at  $k = 0$  (units in millimeters).

time windowed between 55 and 60  $\mu\text{s}$ . Here, we find that the phase of the surface oscillation is nearly identical for all source-to-receiver distances. The magnitude of the Fourier transform of the 30-mm source-to-receiver distance wave form in Fig. 2(c) is shown in Fig. 2(d) and confirms that this oscillation occurs at the coincidence frequency. Unlike conventional resonances, which have zero group velocity at  $k = 0$  and slowly decay (depending on the local curvature) as energy in the vicinity of  $k = 0$  propagates to the far field, waves excited at the conical point at  $k = 0$  propagate from the source with a finite group velocity producing a uniform oscillation over the sample surface. Analogous behavior has been observed in zero index metamaterials [30].

### III. EXPERIMENT SETUP

The experimental approach includes (a) measurements of the Poisson's ratio of plates as a function of temperature to determine the temperature at which the degeneracy ( $\nu = 1/3$ ) occurs and (b) measurements of the dispersion curves and wave fields associated with conical point dispersion. Poisson's ratio was measured using the approach developed by Clorennec *et al.* [6]. This technique allows for very accurate determination of Poisson's ratio independent of the plate thickness. In brief, the sample was excited with a pulsed Nd:YAG laser operating at 532 nm. The resulting transient displacement field was measured on epicenter on the opposite side of the plate using a Michelson interferometer. The displacement field was processed using a fast Fourier transform (FFT) and frequencies corresponding to the  $S_1/S_{2B}$  and  $S_4/S_{5B}$  zero group velocity resonances were identified. The ratio of these two frequencies is uniquely determined by the Poisson's ratio of the plate, and we used a numerical solution of the dispersion equation to determine  $\nu$  based on the measured ZGV frequencies. Note that for the aluminum alloy tested in this work ( $\nu \sim 1/3$ ) we found that the  $S_1/S_{2B}$  and  $S_4/S_{5B}$  frequency ratio yielded more consistent results for  $\nu$  than the  $S_1/S_{2B}$  and  $A_2$  resonance frequency ratio used in previous reports. The temperature dependence of Poisson's ratio was found by cooling the sample

to approximately  $-15^\circ\text{C}$  and taking continuous measurements as the sample warmed to room temperature. The temperature near the excitation and detection laser positions on the sample surface was monitored using a thermocouple. Several aluminum alloys of different compositions and heat treatments were tested at room temperature to determine the material with  $\nu$  closest to  $1/3$ .

Conical dispersion was evaluated using the experimental setup outlined in Fig. 3. Lamb waves were generated by a contact longitudinal wave transducer (Olympus v109) with an aperture of 12.7 mm coupled to the sample with a thin oil layer. The transducer was driven by a function generator coupled to a power amplifier. The displacement normal to the surface was detected using an adaptive, photorefractive crystal based interferometer based on a bismuth silicon oxide crystal. A 3.0 kHz, 3.0 kV field was applied to the crystal to enhance two-wave mixing gain, and the laser source for the interferometer was a single longitudinal mode frequency doubled Nd:YAG laser with an output of 150 mW. Further details of the interferometer configuration are available in the literature [31]. The turning mirrors on the signal leg of the interferometer were mounted on a two-axis translation stage in order to measure the displacement field over the plate surface. The output of the interferometer was sent through a 1.9 MHz analog high pass filter and recorded on an oscilloscope. For measurements taken below room temperature, the plate was placed in a cooling chamber with transparent walls allowing for detection laser access to the surface. The chamber was cooled using dry ice and the measurements were taken when a thermocouple attached to the sample surface near the measurement point indicated the desired temperature. All of the conical point measurements were performed on a large  $610 \times 305$  mm 6061-O aluminum plate with a thickness of  $1.533 \pm 0.003$  mm. At one end of the plate, a semicircular extrusion was machined into the plate edge for experiments demonstrating the spatial invariance of conical point Lamb waves.

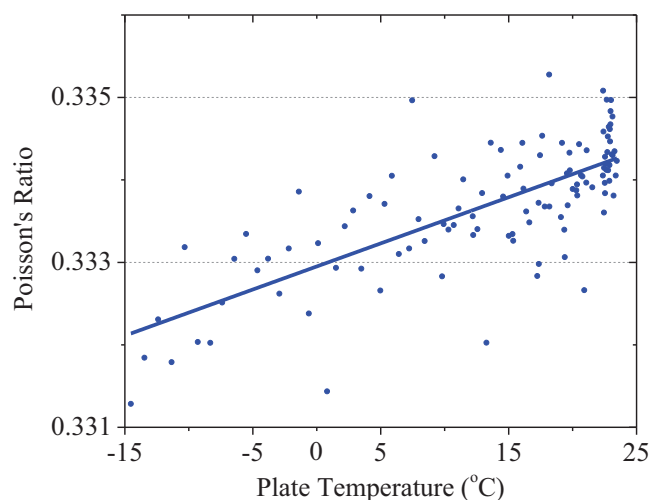


FIG. 4. Measurements of Poisson's ratio as a function of temperature for a 6061-O aluminum plate. The solid line shows a linear fit of the data.

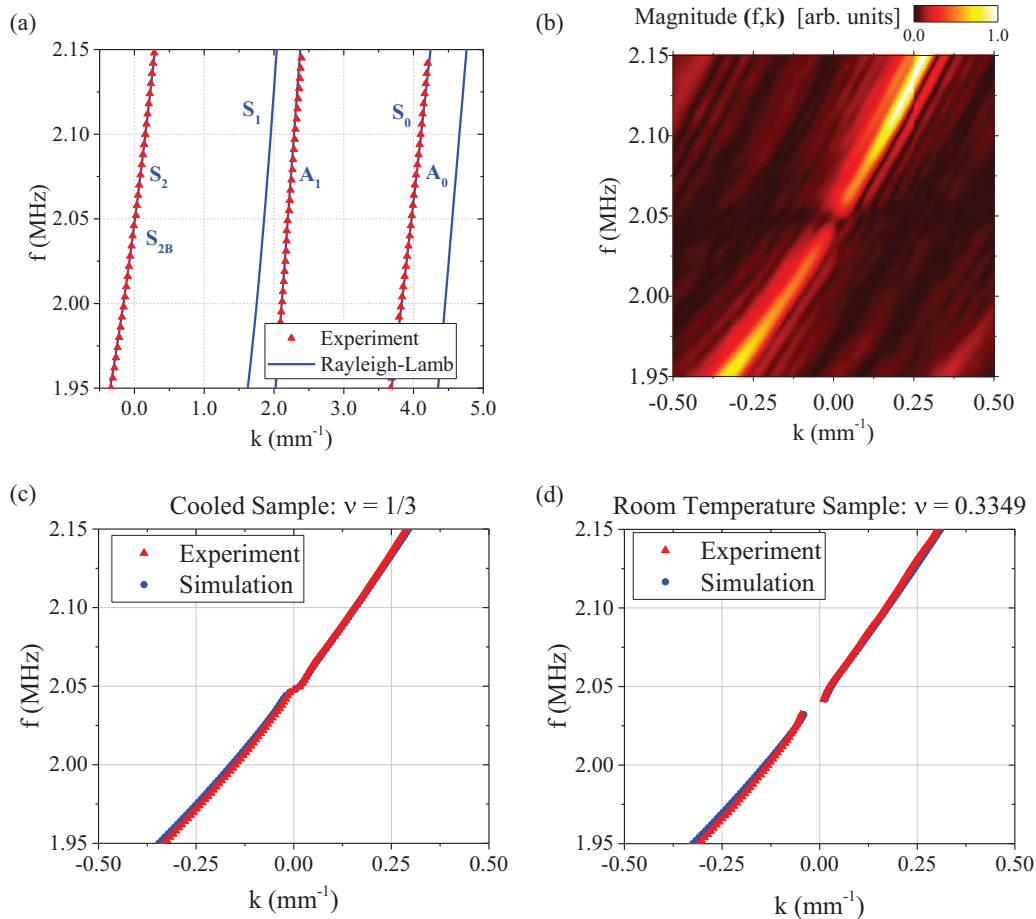


FIG. 5. (a) Measured and calculated dispersion curves for a 6061-O aluminum plate cooled to achieve accidental degeneracy. (b) Magnitude plot of the 2D Fourier transform of the experimentally measured wave forms showing the temporal frequency as a function of spatial frequency in the vicinity of  $k = 0$ . (c) Comparison of dispersion curve found using the experimental data on the cooled plate with that found using a finite difference time domain simulation of the experiment for the degenerate case ( $\nu = 1/3$ ). (d) The same as (c) but using room-temperature measurements and plate properties ( $\nu = 0.3349$ ).

#### IV. EXPERIMENTAL RESULTS AND DISCUSSION

Conical dispersion exists in isotropic plates for discrete values of the material parameters. In this paper, we focus on the lowest order degeneracy that occurs if  $c_1 = 2c_2$  or, equivalently,  $\nu = 1/3$ . This precise condition is not easy to achieve with naturally occurring materials, but many aluminum alloys do, in fact, have a Poisson's ratio very close to  $1/3$ . We performed systematic measurements on commercially available aluminum alloys and found that the alloy 6061-O had a room-temperature Poisson's ratio of  $\nu = 0.3349 \pm 0.0006$ , where standard deviation was found through multiple measurements at different locations on the plate. In order to tune the Poisson's ratio, we take advantage of the temperature-dependent elastic properties and cool the plate. Figure 4 shows the Poisson's ratio measured as a function of temperature at a single location on the plate. A linear fit of this data indicates Poisson's ratio changes by  $\Delta\nu = 5.6 \times 10^{-5}/^\circ\text{C}$  (close to the reported value for pure aluminum of  $\Delta\nu = 5.4 \times 10^{-5}/^\circ\text{C}$  [32]). Given that the room-temperature values of Poisson's ratio were taken at a temperature of  $23^\circ\text{C}$ , and the average Poisson's ratio measured across the sample is  $\nu = 0.3349$ , we expect a Poisson's ratio

of close to  $1/3$  at a measurement temperature of  $-5^\circ\text{C}$ . We can thus tune the plate properties over a reasonable range to achieve the desired degeneracy. Note that there is some spatial variation in Poisson's ratio and we have used the average value measured at room temperature to determine the temperature at which degeneracy occurs. Figure 4, for example, indicates that at this particular point on the plate a Poisson's ratio of  $1/3$  occurs at a temperature closer to  $0^\circ\text{C}$ .

In order to deduce the behavior of conical dispersion, the plate was cooled to  $-5^\circ\text{C}$ , and time domain signals were collected as the source-to-receiver distance was increased in  $250 \mu\text{m}$  steps for a total distance of  $150 \text{ mm}$ , starting  $30 \text{ mm}$  away from the center of the transducer excitation source. The transducer was driven by a five-cycle sine wave at  $2.04 \text{ MHz}$ , near the expected coincidence frequency. The measured wave forms, providing the temporal response as a function of distance, were processed with a two-dimensional FFT giving the temporal frequency as a function of spatial frequency. The dispersion curve shown in Fig. 5(a) was found by extracting the peak values from the magnitude of the two-dimensional (2D) FFT. A smooth transition between the  $S_2$  and  $S_{2B}$  modes is observed at  $k = 0$ . While the large aperture

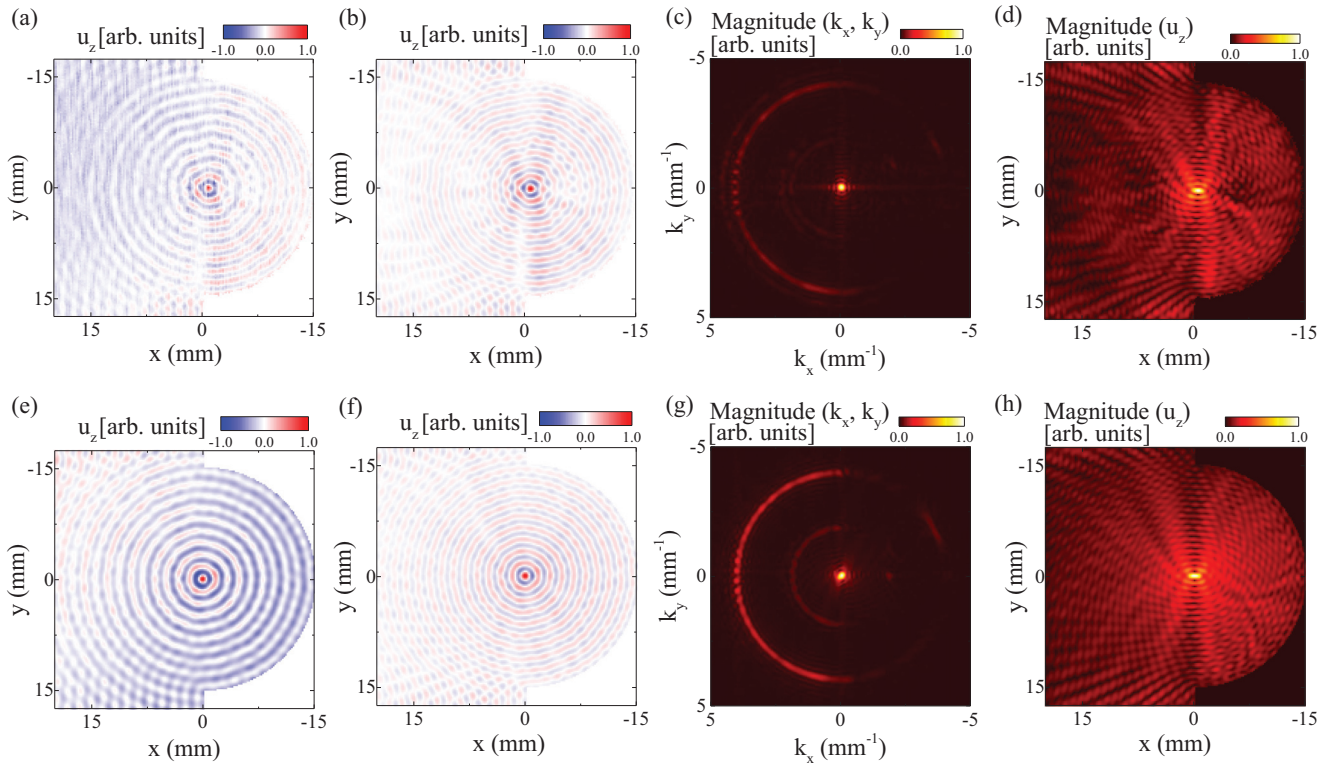


FIG. 6. (a) Out-of-plane displacement at a frequency of  $f = 2.051$  MHz found from the experimental measurements. (b) The displacement field in (a) after a bandpass filter ( $k = 3.0$  to  $5.0$   $\text{mm}^{-1}$ ) in order to isolate the  $S_0$  mode arising from mode conversion at the plate edge. (c) Fourier domain representation of the measured wave field. The dominant modes are the incident  $S_2$  mode near  $k = 0$  and mode converted  $S_0$  mode. (d) Magnitude of the out-of-plane displacement field at 2.051 MHz showing focusing of the  $S_0$  wave field at the center of the lens. (e)–(h) show finite difference simulations of the experiments (with  $\nu = 1/3$ ) and correspond to (a)–(d) above.

transducer does not excite high spatial frequency modes very efficiently, we are still able to detect the  $A_1$  and  $S_0$  modes in the plate while the  $S_1$  and  $A_0$  modes are below the noise level. The solid lines show the dispersion curves calculated from the Rayleigh-Lamb dispersion relation, where Poisson's ratio is taken as  $1/3$ , the cooled plate thickness is  $1.532$  mm, and the shear wave velocity was found to be  $3.138$  mm/ $\mu\text{s}$  through a best fit with the experimental results. The agreement between the experimental and calculated dispersion curves for all of the measured modes is excellent. Figure 5(b) shows the magnitude of the 2D FFT in the vicinity of  $k = 0$ . The magnitude of the response decreases sharply through  $k = 0$  in general agreement with the results of Fig. 2(b). Nevertheless, near-linear dispersion is confirmed for this case of accidental degeneracy and exceptionally long-wavelength propagating waves are detected.

The dispersion curves near  $k = 0$  measured on the cooled sample and the same sample at room temperature are given in Figs. 5(c) and 5(d), respectively. The room-temperature sample is very close to degeneracy, but the response falls below the noise level at very small  $k$  values. This gap in  $k$  is due to the fact that parabolic dispersion in this case leads to very small group velocity for small  $k$  and thus these waves are not detected over the measurement time. In addition, the lower branch is associated with a shear thickness mode resonance that has little out-of-plane displacement in the vicinity of  $k = 0$ . The curve measured on the cooled sample shows a continuous transition from forward to backward wave

propagation. However, there is a small distortion, or break from linear behavior, observed for very small  $k$  values. In order to better understand this, we also simulated the experiments using the finite difference time domain software PZFLEX. In the simulation, we used a circular normal forcing function with a diameter matching the transducer diameter, and all other parameters matching those used in the experiment. In addition, the data was processed using the same approach used for the experimental measurements. The dispersion curves from the simulations are also shown in Figs. 5(c) and 5(d) and agree well with the experimental measurements. Both simulation and experiment show similar behavior for small  $k$  values. Additional simulations in PZFLEX show this distortion is reduced as the distance from the source to the detection points is increased, indicating that it is associated with operation in the near field of the source.

One of the peculiar features of conical point Lamb waves is that they propagate with an infinite wavelength. This essentially decouples the spatial and temporal behavior and leads to a surface displacement that oscillates in time but is fixed in space. A direct consequence of this is that the concept of propagation direction loses significance. In order to demonstrate this behavior experimentally, we machined a 30-mm-diameter semicircle on the edge of the aluminum plate. The transducer is positioned at a randomly selected position far from the semicircle, at the location indicated in Fig. 3. The experiments were performed at room temperature where near degeneracy occurs. The transducer was driven with a

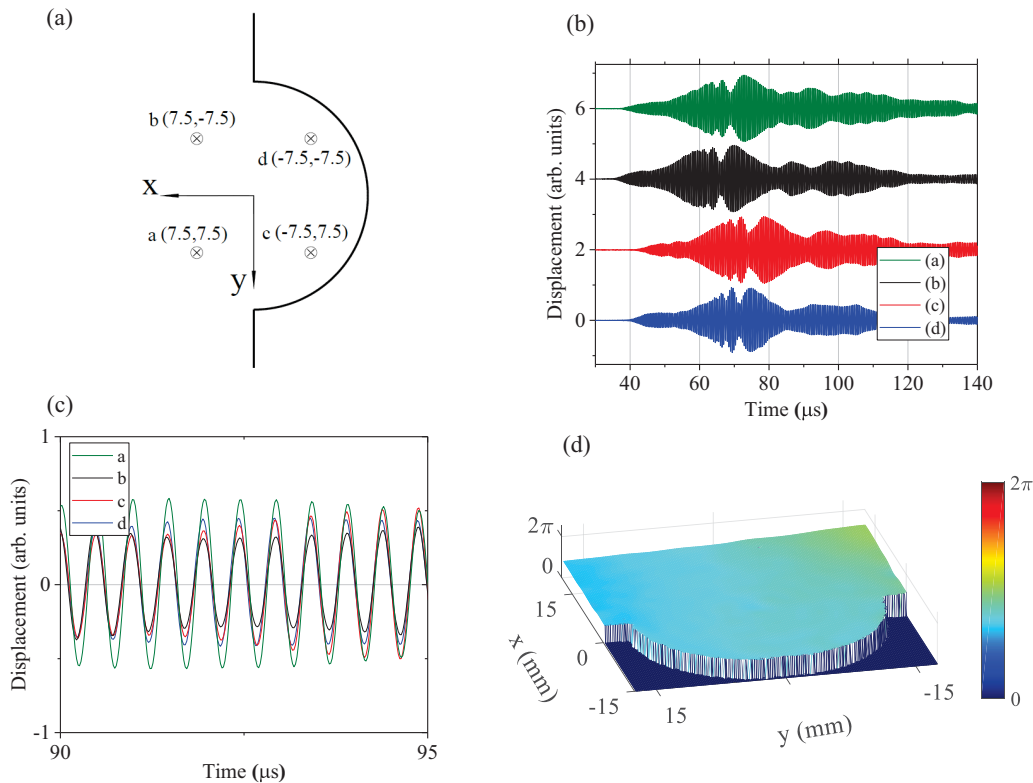


FIG. 7. (a) Four locations on the plate surface near the semicircle where temporal responses are inspected. (b) Time domain responses after a low-pass spatial filter ( $k = 1.0 \text{ mm}^{-1}$ ), in order to isolate the  $S_2$  mode, at the four locations shown in (a). (c) Zoomed-in view of the time domain responses in (b) showing the uniform phase of the oscillations at the different spatial positions. (d) Phase of the oscillation of the  $S_2$  mode over the surface of the lens at 2.051 MHz. A low-pass spatial filter ( $k = 1.0 \text{ mm}^{-1}$ ) was used to isolate the  $S_2$  mode.

50-cycle tone burst at a frequency of 2.051 MHz, where the spatial frequency is quite close to zero. This gives a wavelength of 220 mm and an associated phase velocity of  $4.5 \times 10^3 \text{ m/s}$  [see Fig. 1(b)]. The detection laser was scanned over a  $35 \times 35 \text{ mm}^2$  region of the plate, encompassing the semicircular feature, with a step size of 0.2 mm along each axis, and the out-of-plane surface displacement was measured at each spatial position.

The time domain wave forms were windowed between 60 and  $100 \mu\text{s}$  and processed using a Fourier transform. The magnitude and phase angle of the surface displacement at a frequency of 2.051 MHz was determined at each spatial position, and the displacement amplitude is plotted in Fig. 6(a). Note that the near-degenerate  $S_2$  mode has a wavelength much larger than the image size, resulting in a dc offset to the image but contributing little spatial structure. The main feature in Fig. 6(a) is the  $S_0$  mode, with a wavelength of 1.57 mm, which is produced by mode conversion of the  $S_2$  mode at the plate edge. Figure 6(b) shows the same data as in Fig. 6(a), but spatially filtered between  $k = 3.0$  and  $5.0 \text{ mm}^{-1}$  to better observe the  $S_0$  wave field. The mode converted wave has an angle of reflection of (very close to) zero degrees irrespective of the angle of incidence, leading to focusing of the mode converted wave field by the semicircular extrusion. Furthermore, this type of lens will focus the mode converted field regardless of the position of the  $S_2$  mode excitation source on the plate surface. Figure 6(c) shows the 2D FFT

of the complex data at 2.051 MHz. The bright spot near  $k = 0$  corresponds to the  $S_2$  mode, while the semicircular ring corresponds to the  $S_0$  mode produced at the plate edge through the mode conversion. The magnitude of the  $S_0$  field is quite uniform over the full  $180^\circ$  defined by the semicircular edge. The magnitude of the displacement field at 2.051 MHz is shown in Fig. 6(d), where clear focusing at the center of curvature of the lens is observed.

The experimental measurement was taken at room temperature where a near degeneracy occurs. In order to investigate potential differences in the wave field behavior that could occur at a true accidental degeneracy, we simulated the experimental measurement using PZFlex and taking a Poisson's ratio of 1/3. The source was again taken as a circular normal force with a diameter matching that of the transducer, and the mechanical properties were selected to match the cooled specimen discussed earlier in the paper. The temporal excitation profile and data processing approach match those in the experiment. In this case, the degeneracy occurs at a frequency of 2.048 MHz. Figures 6(e) and 6(f) give the calculated displacement field and bandpass filtered displacement field, respectively. Figures 6(g) and 6(h) show the calculated spatial FFT and displacement magnitude plot, respectively. A qualitative comparison between all experimental and simulated plots shows reasonable agreement between the two. In particular, both show angle independent mode conversion and normal reflection for the  $S_0$  mode at the

free edge over the full  $180^\circ$  surface of the semicircular extrusion.

We further investigate the wave field for near-conical dispersion by examining the time domain responses at the positions in the lens indicated in Fig. 7(a). The data was low-pass filtered at a spatial frequency of  $1.0 \text{ mm}^{-1}$  in order to isolate the  $S_2$  mode and the resulting wave forms are shown in Fig. 7(b). The traces show an initial transient tone burst, similar to that seen in Fig. 2(a), followed by a prolonged ringing. Figure 7(c) shows zoomed-in wave forms between 90 and 95  $\mu\text{s}$ . The surface displacement at all four of these points oscillates with a nearly identical phase, as expected due to the unusually large wavelength of the  $S_2$  mode. The wavelength of the  $S_2$  mode at 2.051 MHz was estimated by inspecting the phase delay of the displacement response and was found to be 190 mm, with an associated phase velocity of  $3.9 \times 10^5 \text{ m/s}$ . Figure 7(d) shows the phase angle of the displacement response at 2.051 MHz. The data was spatially low-pass filtered ( $k = 1.0 \text{ mm}^{-1}$ ) and the phase angle found by using a temporal FFT of the wave forms in the 60–100  $\mu\text{s}$  time window. Waves excited in this near-degenerate case produce a field that is remarkably uniform in phase over the surface of the lens.

## V. CONCLUSIONS

Conical dispersion at finite frequencies and zero wave number produces propagating waves that have an infinite

wavelength. In practice, this leads to elastic waves that travel away from a particular source with a finite group velocity while maintaining a uniform phase at each point in space, producing a field that can be considered in some sense static in space, yet still oscillating in time. While there has been a substantial amount of interest in the development of optical and acoustic media that support conical dispersion at  $k = 0$ , generally referred to as zero index media [23,30], conical dispersion in homogeneous isotropic waveguides has received limited attention. Here we demonstrate that conical dispersion can be achieved by tuning the Poisson's ratio of an elastic plate such that accidental degeneracy between a longitudinal and transverse thickness mode resonance of the same symmetry occurs. We confirm through both computation and experiment that Lamb waves generated at the conical point frequency show a uniform phase over the plate surface. Furthermore, we show that these waves exhibit angle independent mode conversion upon encountering the free edge of the plate. Future studies will explore the scattering of conical point Lamb waves at plate defects and look toward applications for these waves in the nondestructive evaluation of materials and the development of acoustic devices.

## ACKNOWLEDGMENT

The authors gratefully acknowledge the support of this research by the National Science Foundation under Grant No. CMMI 1335426.

- 
- [1] J. L. Rose, *Ultrasonic Waves in Solid Media* (Cambridge University Press, New York, 1999).
  - [2] J. D. Achenbach, *Wave Propagation in Elastic Solids* (North-Holland, Amsterdam, 1973).
  - [3] I. Tolstoy and E. Usdin, Wave propagation in elastic plates: Low and high mode dispersion, *J. Acoust. Soc. Am.* **29**, 37 (1957).
  - [4] A. H. Meitzler, Backward-wave transmission of stress pulses in elastic cylinders and plates, *J. Acoust. Soc. Am.* **38**, 835 (1965).
  - [5] C. Prada, O. Balogum, and T. W. Murray, Laser-based ultrasonic generation and detection of zero-group velocity Lamb waves in thin plates, *Appl. Phys. Lett.* **87**, 194109 (2005).
  - [6] D. Clorennec, C. Prada, and D. Royer, Local and noncontact measurements of bulk acoustic wave velocities in thin isotropic plates and shells using zero group velocity Lamb modes, *J. Appl. Phys.* **101**, 034908 (2007).
  - [7] C. Prada, D. Clorennec, and D. Royer, Simulation and measurement of the optical excitation of the  $S_1$  zero group velocity Lamb wave resonance in plates, *J. Appl. Phys.* **102**, 064914 (2007).
  - [8] C. Prada, D. Clorennec, and D. Royer, Local vibration of an elastic plate and zero-group velocity Lamb modes, *J. Acoust. Soc. Am.* **124**, 203 (2008).
  - [9] S. Mezil, J. Laurent, D. Royer, and C. Prada, Non contact probing of interfacial stiffness between two plates by zero-group velocity Lamb modes, *Appl. Phys. Lett.* **105**, 021605 (2014).
  - [10] S. Bramhavar, C. Prada, A. A. Maznev, A. G. Every, T. B. Norris, and T. W. Murray, Negative refraction and focusing of elastic Lamb waves at an interface, *Phys. Rev. B* **83**, 014106 (2011).
  - [11] F. D. Philippe, T. W. Murray, and C. Prada, Focusing on plates: Controlling guided waves using negative refraction, *Sci. Rep.* **5**, 11112 (2015).
  - [12] M. Germano, A. Alippi, A. Bettucci, and G. Mancuso, Anomalous and negative reflection of Lamb waves in mode conversion, *Phys. Rev. B* **85**, 012102 (2012).
  - [13] I. A. Veres, C. Grunsteidl, D. M. Stobbe, and T. W. Murray, Broad angle negative reflection and focusing of elastic waves from a plate edge, *Phys. Rev. B* **93**, 174304 (2016).
  - [14] B. Gerardin, J. Laurent, C. Prada, and A. Aubry, Negative reflection of Lamb waves at a free edge: Tunable focusing and mimicking phase conjugation, *J. Acoust. Soc. Am.* **140**, 591 (2016).
  - [15] M. Ibanescu, S. G. Johnson, D. Roundy, C. Luo, Y. Fink, and J. D. Joannopoulos, Anomalous Dispersion Relations by Symmetry Breaking in Axially Uniform Waveguides, *Phys. Rev. Lett.* **92**, 063903 (2004).
  - [16] T. J. Delph, G. Herrmann, and R. K. Kaul, On coalescence of frequencies and conical points in the dispersion spectra of elastic bodies, *Int. J. Solids Struct.* **13**, 423 (1977).
  - [17] R. D. Mindlin, *An Introduction to the Mathematical Theory of Vibrations of Elastic Plates* (World Scientific, Singapore, 2016).
  - [18] X. Huang, Y. Lai, Z. H. Hang, H. Zheng, and C. T. Chan, Dirac cones induced by accidental degeneracy in photonic crystals and zero-refractive-index materials, *Nat. Mater.* **10**, 582 (2011).
  - [19] F. Liu, Y. Lai, X. Huang, and C. T. Chan, Dirac cones at  $k = 0$  in phononic crystals, *Phys. Rev. B* **84**, 224113 (2011).



- [20] M. Silveirinha and N. Engheta, Tunneling of Electromagnetic Energy through Subwavelength Channels and Bends using  $\epsilon$ -Near-Zero Materials, *Phys. Rev. Lett.* **97**, 157403 (2006).
- [21] R. Liu, Q. Cheng, T. Hand, J. J. Mock, T. J. Cui, S. A. Cummer, and D. R. Smith, Experimental Demonstration of Electromagnetic Tunneling Through an Epsilon-Near-Zero Metamaterial at Microwave Frequencies, *Phys. Rev. Lett.* **100**, 023903 (2008).
- [22] J. Hao, W. Yan, and M. Qiu, Super-reflection and cloaking based on zero index metamaterial, *Appl. Phys. Lett.* **96**, 101109 (2010).
- [23] F. Liu, X. Huang, and C. T. Chen, Dirac cones at  $k = 0$  in acoustic crystals and zero index acoustic materials, *Appl. Phys. Lett.* **100**, 071911 (2012).
- [24] V. C. Nguyen, L. Chen, and K. Halterman, Total Transmission and Total Reflection by Zero Index Metamaterials with Defects, *Phys. Rev. Lett.* **105**, 233908 (2010).
- [25] Q. Wei, Y. Cheng, and X. Liu, Acoustic total transmission and total reflection in zero-index metamaterials with defects, *Appl. Phys. Lett.* **102**, 174104 (2013).
- [26] F. Liu and Z. Liu, Elastic Waves Scattering without Conversion in Metamaterials with Simultaneous Zero Indices for Longitudinal and Transverse Waves, *Phys. Rev. Lett.* **115**, 175502 (2015).
- [27] A. A. Maznev, Dirac cone dispersion of acoustic waves in plates without phononic crystals, *J. Acoust. Soc. Am.* **135**, 577 (2014).
- [28] A. L. Shuvalov and O. Poncelet, On the backward Lamb waves near thickness resonances in anisotropic plates, *Int. J. Solids Struct.* **45**, 3430 (2008).
- [29] J. B. Spicer, A. D. W. McKie, and J. W. Wagner, Quantitative theory for laser ultrasonic waves in a thin plate, *Appl. Phys. Lett.* **57**, 1882 (1990).
- [30] I. Liberal and N. Engheta, Near zero refractive index photonics, *Nat. Photonics* **11**, 149 (2017).
- [31] A. Blouin and J. P. Monchalain, Detection of ultrasonic motion of a scattering surface by two-wave mixing in photorefractive GaAs crystal, *Appl. Phys. Lett.* **65**, 932 (1994).
- [32] Tables of Physical and Chemical Constants, 16th ed. (Longmans, Green Co., 1995), 2.1.4 Hygrometry. Kaye & Laby Online, Version 1.0 (2005).